Original Paper

phys. stat. sol. (a) **202**, No. 13, 2565–2573 (2005) / **DOI** 10.1002/pssa.200421122

Temperature-dependent stimulated emission cross section and concentration quenching in highly doped Nd^{3+}:YAG crystals

Jun Dong[*, 1, 2], **A. Rapaport**[2], **M. Bass**[2], **F. Szipocs**[2], and **Ken-ichi Ueda**[1]

[1] Institute for Laser Science, University of Electro-Communications, 1-5-1 Chofugaoka, Chofu, Tokyo 182-8585, Japan

[2] School of Optics /CREOL/FPCE, University of Central Florida, Orlando, FL 32816-2700, USA

Received 10 February 2004, revised 29 June 2005, accepted 7 July 2005
Published online 23 August 2005

PACS 42.55.Rz, 42.70.Hj, 78.45.+h, 78.55.Hx

Measurements are reported of the spectroscopic properties (absorption and emission spectra, stimulated emission cross section, and radiative lifetime) of Nd:YAG crystals doped with 1, 2 and 3 at% Nd^{3+} in the temperature range between 70 and 300 K. The stimulated emission cross sections for these crystals were determined using the Füchtbauer–Ladenburg (F–L) formula at each different temperature. The absorption spectra at room temperature were used to calculate the $^4F_{3/2} \rightarrow {}^4I_{11/2}$ stimulated-emission cross section and the $^4F_{3/2}$ radiative lifetime according to Judd–Ofelt theory. As the temperature decreases the emission cross section increases, while the emission lifetime remains constant for all the samples. The temperature dependences of the stimulated emission cross sections for the differently doped crystals are in good agreement with earlier predictions. The concentration quenching effect in highly doped Nd:YAG was also addressed. Although there is concentration quenching in the highly doped Nd:YAG crystals, they are still promising efficient laser materials for high-power microchip solid-state lasers.

1 Introduction

Recent developments of laser diode (LD) pumped solid-state microchip lasers have stimulated the development of high-gain media. Among the high-gain media, Nd-doped yttrium vanadate (Nd:YVO_4) crystal is a suitable material for highly efficient microchip lasers owing to its large absorption coefficient (31.2 cm^{-1} for 1 at% Nd:YVO_4) and large absorption cross section (~25×10^{-19} cm^2) [1]. However, the poor thermal properties and small saturation fluence of Nd:YVO_4 make it unsuitable for high-power operation. The neodymium (Nd) doped yttrium aluminum garnet (YAG) is the most readily available laser material used for microchip lasers and supports a huge area of laser applications because of its combined optical, thermal and mechanical properties. The high-quality Nd:YAG crystal can be obtained by the traditional Czochralski (CZ) method, however, the Nd concentration in Nd:YAG crystal grown by the Czochralski method is relatively low and a longer crystal is required to obtain enough gain, which makes the Nd:YAG crystals grown by the CZ method not suitable for use in microchip lasers. When Nd-doped YAG crystal is grown by the CZ method, yttrium in YAG is substituted by Nd ions. The Nd ion concentration is limited to less than 1.1 at% because the distribution coefficient of Nd in YAG is only 0.18. The high concentration of laser-active ions in a laser crystal absorbs pump power efficiently with short crystal length and this makes the laser system very compact. So, high concentration laser crystals are the goal for development of microchip lasers and many efforts have been taken to search for such high-concentration laser materials. Recently some studies have been reported on highly Nd-doped crystals [2, 3] or ceramics [4, 5], comparing Nd-doped YAG crystals with Nd-doped YAG ceramics, we can

[*] Corresponding author: e-mail: dong@ils.uec.ac.jp, Phone: +81 0424-43-5708, Fax: +81 0424-85-8960

clearly see that Nd:YAG crystals are better than Nd-doped YAG ceramics, because Nd-doped YAG crystal is a single crystal and has a perfect structure, and the structure of Nd-doped YAG ceramics is not perfect, when pump light is inserted into Nd-doped YAG ceramics, there exists scattering, so the absorption of pump power is not efficiently. Therefore, highly Nd-doped YAG single crystal would still be a more suitable laser material in all solid-state age with several fine characteristics that essentially YAG possesses, for instance, relatively long fluorescence lifetime, high thermal conductivity, chemical and physical stability, and other isotropic natures. These characteristics act effectively especially in high-power or pulsed laser operations.

The high-quality Nd:YAG crystals were successfully grown by the temperature gradient technique (TGT) and highly efficient laser operation was obtained by using such highly doped Nd:YAG crystals as gain media [6]. The laser efficiency for 3 at% Nd:YAG is lower than that of 2 at% Nd:YAG, and the threshold pump power for 3 at% Nd:YAG is higher than that of 2 at% Nd:YAG, so there is strong Nd–Nd interaction in the highly doped Nd:YAG crystals, but there is no such report on the effect of concentrations on the spectral properties and emission quenching. Here, we present the effects of Nd concentration and temperature on the stimulated emission cross section and fluorescence lifetime to elucidate the possible mechanisms involved in the Nd^{3+} concentration quenching in highly doped Nd:YAG crystals.

2 Experiments

Highly doped Nd:YAG crystals (up to 3 at% Nd) were grown by temperature gradient technology (TGT) successfully, the growth parameters are described in detail in [6]. Samples doped with 1, 2 and 3 at% Nd^{3+} for spectroscopic and lifetime measurements were cut from the boules and the surfaces perpendicular to the ⟨111⟩ growth axis were polished. The samples were 2 mm thick.

The room-temperature absorption spectra were measured using a Cary 500 Scan UV-Vis-NIR spectrophotometer. Emission spectra were measured between 850 nm and 1500 nm with a fiber-coupled diode laser operating at 808 nm. Nd^{3+} ions were pumped into their $^4F_{3/2}$ states from which they relaxed to the ground $^4I_{11/2}$ state. The excitation signal was monitored during the experiment with a silicon (Si) detector. An indium gallium arsenide (InGaAs) detector located at the output slit of a 25 cm focal length Jarell–Ash monochromator was used to detect the fluorescence emission intensity. With 50 μm slits the resolution of this detection system was about 0.4 nm. Prior to use in calculating the stimulated emission cross section, the recorded spectra were corrected for the spectral response of the detector and of the monochromator grating. Calibration of the detection system was achieved by recording its response to light from a tungsten-iodine white light source that had been calibrated at the National Institute for Standards and Testing (NIST).

The emission lifetime measurements employed excitation from a tunable optical parametric oscillator set to 808 nm (e.g. Quanta Ray MOPO-SL) that was itself pumped by the third harmonic of a Q-switched Nd:YAG laser. The OPO's linewidth was ~0.2 cm^{-1} and its pulse duration was ~5 ns. The energy of the idler pulse at 808 nm is less than 2 mJ. Fluorescence was collected with a 5 cm focal length lens and spectrally dispersed with the monochromator. An InGaAs photodiode connected to a preamplifier was used to detect the fluorescence and monitor its decay with time. Decay curves were recorded using a Tektronix 2440 500 Ms/s digital oscilloscope and computer-controlled data-acquisition system. The emission spectra and lifetime measurements were carried out at temperatures from 70 to 300 K in a temperature-controlled compressed-helium cryostat.

3 Results and discussion

All the absorption band shapes and their wavelengths are found to be the same except for differences in the measured strengths resulting from the different Nd^{3+} concentrations in Nd^{3+}:YAG crystals. The second maximum absorption band in the 300–1000 nm wavelength range is centered at 808 nm (as shown in Fig. 1 for 2 at% Nd:YAG crystal at room temperature) where commercial laser diodes are available as pump sources. With increasing Nd^{3+} concentration, the absorption coefficient at 808 nm increases from about 7 cm^{-1} for 1 at% Nd^{3+} concentration to 20.8 cm^{-1} for 3 at%, which is shown in the inset of Fig. 1.

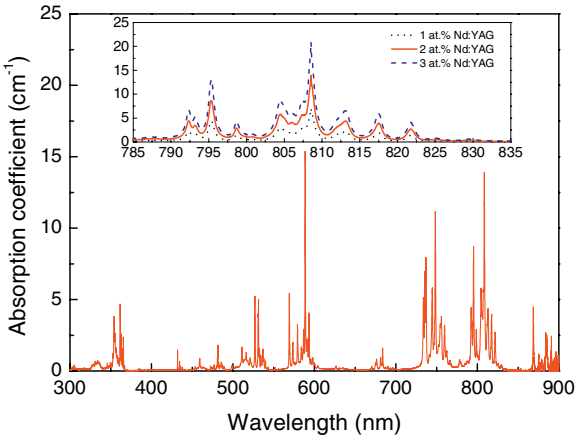

Fig. 1 (online colour at: www.pss-a.com) Absorption spectra of 2 at% Nd^{3+} doped Nd:YAG crystals at room temperature, the inset is the absorption spectra of Nd:YAG crystal with different Nd^{3+} concentrations around the wavelength range from 785 nm to 835 nm.

The fluorescence spectra of Nd:YAG crystals doped with 1, 2 and 3 at% Nd at room temperature are shown in Fig. 2, nearly indentical emission structure for three different concentrations of Nd:YAG crystal at room temperature can be seen, the peak emisson wavelength is centered at 1064 nm.

The measured room-temperature absorption spectra of Nd:YAG crystals from Fig. 1 were used to find the oscillator strength of each line for each Nd:YAG crystal studied according to Judd–Ofelt theory [7, 8]. The experimental line oscillator strength caused by the transition of the electronic dipole was calculated using the following equation [9]:

$$S = \frac{3hc(2J+1)}{8\pi^3 e^2 \bar{\lambda} N_0} \frac{9n}{(n^2+2)^2} \int \alpha(\lambda)\, \mathrm{d}\lambda, \tag{1}$$

where $\alpha(\lambda) = 2.303 D_0/d$ is the absorption coefficient at a given wavelength λ and $D_0(\lambda)$ is the optical density ($\log I_0/I$), $\bar{\lambda}$ is the mean wavelength of the specific absorption band, d is the thickness of the sample in cm, e is the electric charge, N_0 is the number density of Nd^{3+}, n is the refractive index and assumed concentration independent, c the velocity of light, h is the Planck constant, J the total angular

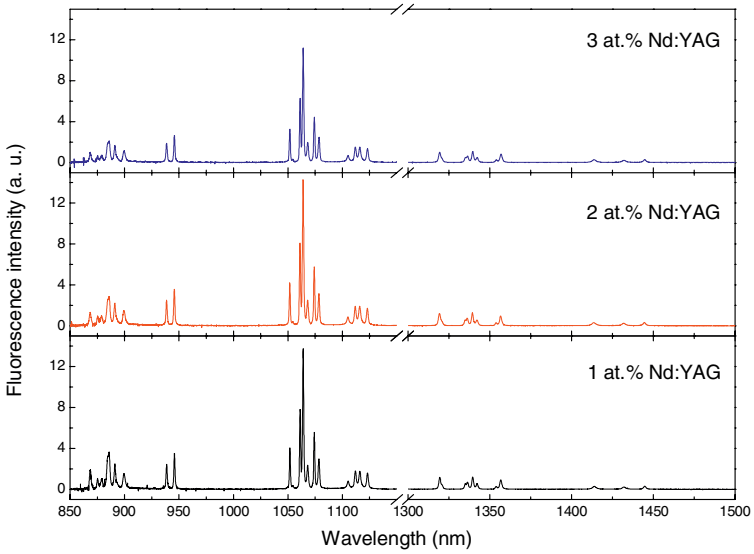

Fig. 2 (online colour at: www.pss-a.com) Fluorescence spectra of Nd:YAG crystals doped with 1, 2 and 3 at% Nd at room temperature from 850 nm to 1500 nm.

momentum of the ground state ($J = \frac{9}{2}$ for Nd^{3+}), and S is the line oscillator strength of an electric dipole transition, defined as

$$S = \sum_{t=2,4,6} \Omega_t \left| \langle (S, L)\, J \| U^t \| (S', L')\, J' \rangle \right|^2, \tag{2}$$

where $\|U^t\|$ is the doubly reduced matrix elements of the unit tensor operator of rank $t = 2$, 4 and 6 that are calculated from the intermediate coupling approximation. The three phenomenological Judd–Ofelt parameters Ω_2, Ω_4 and Ω_6 exhibit the influence of the host on the radiative transition probabilities, since they contain implicitly the effect of the odd-symmetry crystal field terms, interconfigurational radial integrals and energy denominators.

The values of S_{exp} obtained by the numerical integration of the absorption line shapes according to Eq. (1) are given in Table 1. This shows that the values of oscillator strength of various absorption bands are almost independent of the Nd concentrations in YAG crystals.

The oscillator strength parameters Ω_2, Ω_4 and Ω_6 can be derived by a computerized least-squares fitting of the experimental oscillator strength with Eq. (2). The values of the doubly reduced matrix elements of the unit tensor operator for these absorption bands were taken from the set of values of Nd^{3+} listed by Kaminskii [10], since the reduced matrix elements exhibit only small variations with the host lattice [11]. The best set of Ω_t parameters of each Nd:YAG crystal are listed in Table 2 along with the spectroscopic quality factor Q. These results are in good agreement with those previously reported for the Nd^{3+} ion in YAG crystals [12]. The quality of the fitting can be expressed by the minimum root-mean-square (rms) deviation in the oscillator strengths between the calculated S_{cal} and the measured S_{exp} values, which is defined as [10]

$$\Delta S_{rms} = \left[\frac{\sum (S_{cal} - S_{exp})^2}{q - p} \right]^{1/2}, \tag{3}$$

where q is the number of analyzed line groups (intermultiplet transitions) and p is the number of parameters sought, which in our case is three. The rms deviations of the oscillator strengths for different concen-

Table 1 Measured and calculated line strengths ($\times 10^{-20}$ cm^2) of Nd:YAG crystals having different Nd^{3+} concentrations.

λ (nm)	excited state	1 at%		2 at%		3 at%	
		S_{exp}	S_{cal}	S_{exp}	S_{cal}	S_{exp}	S_{cal}
875	$^4F_{3/2}$	0.356	0.706	0.359	0.682	0.364	0.665
808	$^2H_{9/2}$, $^4F_{5/2}$	2.663	2.691	2.657	2.651	2.554	2.601
748	$^4S_{3/2}$, $^4F_{7/2}$	2.536	2.518	2.482	2.495	2.492	2.453
684	$^4F_{9/2}$	0.303	0.256	0.291	0.254	0.29	0.249
626	$^2H_{11/2}$	0.037	0.065	0.035	0.064	0.035	0.063
588	$^4G_{5/2}$	1.455	1.461	1.451	1.458	1.445	1.449
569	$^2G_{7/2}$	0.398	0.542	0.399	0.526	0.396	0.515
527	$^4G_{7/2}$, $^2K_{13/2}$	0.813	0.620	0.698	0.605	0.7	0.592
516	$^4G_{9/2}$	0.488	0.366	0.593	0.360	0.49	0.354
482	$^2K_{15/2}$, $^2G_{9/2}$, $^2D_{3/2}$	0.28	0.106	0.265	0.104	0.268	0.102
459	$^4G_{11/2}$	0.216	0.055	0.209	0.054	0.195	0.053
432	$^2P_{1/2}$	0.09	0.062	0.082	0.059	0.083	0.057
385	$^2P_{3/2}$	0.0015	0.007	0.0016	0.007	0.022	0.006
354	$^4D_{3/2}$, $^4D_{5/2}$	0.8	0.431	0.75	0.412	0.768	0.500
346	$^2I_{11/2}$, $^4D_{1/2}$	0.064	0.047	0.06	0.046	0.08	0.045
	ΔS_{rms}		0.127		0.121		0.126

Table 2 Judd–Ofelt parameters of the Nd:YAG crystals with different Nd concentrations.

	1 at%	2 at%	3 at%
Ω_2 (10^{-20} cm^2)	0.623	0.664	0.68
Ω_4 (10^{-20} cm^2)	1.698	1.605	1.554
Ω_6 (10^{-20} cm^2)	5.762	5.717	5.623
$Q = \Omega_4/\Omega_6$	0.29	0.28	0.28
n	1.82	1.82	1.82
N_0 (10^{20} ions/cm^3)	1.38	2.76	4.14

tration Nd:YAG crystals are also presented in Table 1, which are about 10% of the average line strengths for Nd:YAG crystals doped with different concentrations.

The radiative lifetime was determined by the following equation according to Judd–Ofelt theory [7, 8]:

$$\tau_{\mathrm{rad}} = A_{\mathrm{T}}^{-1} = \frac{1}{\sum\limits_{S', L', J'} A_{\mathrm{rad}}[(S', L')\, J'; (S, L)\, J]}\,, \tag{4}$$

where A_{T} is the total radiative transition probability, A_{rad} is the radiative transition probability from the initial J' manifold $(S', L')\, J'$ to the terminal manifold $(S, L)\, J$, and A_{rad} can be determined by using the Ω_t parameters according to the expression:

$$A_{\mathrm{rad}}[(S', L')\, J'; (S, L)\, J] = \frac{64\pi^4}{3h(2J+1)\,\bar{\lambda}^3}\left[\frac{n(n^2+2)^2}{9}\, S_{\mathrm{ed}} + n^3 S_{\mathrm{md}}\right], \tag{5}$$

where $n(n^2 + 2)^2/9$ is the local field correction for Nd^{3+} in the initial manifold, n is the refractive index of the medium, S_{ed} and S_{md} represent the line strengths for the induced electric and magnetic dipole transition, respectively, which are expressed by

$$S_{\mathrm{ed}} = e^2 \sum_{t=2,4,6} \Omega_t \left|\left\langle (S', L')\, J' \middle\| U^t \middle\| (S, L)\, J \right\rangle\right|^2 \tag{6}$$

$$S_{\mathrm{md}} = \left(\frac{e^2h^2}{16\pi^2m^2c^2}\right)\left|\left\langle (S, L)\, J \middle\| L + 2S \middle\| (S', L')\, J' \right\rangle\right|^2. \tag{7}$$

The fluorescence branching ratio β can be obtained by using the values of the radiative transition probability (A_{rad}) from the expression:

$$\beta[(S, L)\, J; (S', L')\, J'] = \frac{A_{\mathrm{rad}}[(S', L')\, J'; (S, L)\, J]}{\sum\limits_{S', L', J'} A_{\mathrm{rad}}\,[(S', L')\, J'; (S, L)\, J]}\,. \tag{8}$$

The radiative transition probabilities and branching ratios for the fluorescence from the $^4F_{3/2}$ to the ^4I_J states are listed in Table 3.

Table 3 Calculated radiative properties of Nd^{3+} ion in YAG crystals.

$^4F_{3/2}$ to	1 at%			2 at%			3 at%		
	A (s^{-1})	β (%)	A_{T} (s^{-1})	A (s^{-1})	β (%)	A_{T} (s^{-1})	A (s^{-1})	β (%)	A_{T} (s^{-1})
$^4I_{15/2}$	27	0.6	3995	26	0.7	3924	26	0.7	3892
$^4I_{13/2}$	536	13.4		532	13.5		527	13.5	
$^4I_{11/2}$	2303	57.6		2275	58		2255	57.9	
$^4I_{9/2}$	1129	28.4		1091	27.8		1084	27.9	

Table 4 Room-temperature emission properties of Nd^{3+} in YAG crystals with different Nd concentrations.

Sample	λ (nm)	$\Delta\lambda$ (nm)	τ_R (μs)	τ_{exp} (μs)
1 at% Nd	1064	1.3	250	228
2 at% Nd	1064	1.4	255	145
3 at% Nd	1064	1.4	256	128

The radiative lifetimes τ_R for the $^4F_{3/2} \rightarrow {}^4I_{11/2}$ transition determined by using Judd–Ofelt theory are presented in Table 4 together with the effective fluorescence linewidth that was determined from the fluorescence spectra of Nd:YAG crystal doped with different concentrations of Nd at room temperature, as shown in Fig. 2. The radiative lifetimes are nearly the same for the different Nd^{3+} concentrations in Nd:YAG crystals; about 255 μs. The difference of the radiative lifetime for the different Nd concentrations is caused by the calculation measurement error and the radiative lifetime (250 μs) calculated by the Judd–Ofelt theory for 1 at% Nd:YAG is in a good agreement with the value published for a very low concentration Nd:YAG sample [13].

The fluorescence decay of each sample studied was mainly exponential and could be fitted at late times with a single exponential function. However, in these highly Nd-doped samples, a slightly faster decay at early time that can be explained by the concentration quenching [14] was observed. In the case of higher doping concentrations of Nd:YAG crsytal, an effective lifetime can be defined as follows [14, 15]:

$$\tau_{eff} = \int_0^\infty \frac{I(t)}{I_0}\,\mathrm{d}t, \tag{9}$$

where I_0 is the initial emission intensity. The nonexponential emission decay behavior of three doping concentration Nd:YAG crystals at room temperature is shown in Fig. 3, the decay is fitted logarithmically for each sample at room temperature according to the formula [14] that includes the effect of cross-relaxation and the energy migration on the luminescence quenching:

$$I(t) = I_0 \exp\left(-\frac{t}{\tau_{rad}} - \frac{t}{\tau_D} - \gamma\left(\frac{t}{\tau_{rad}}\right)^{1/2}\right), \tag{10}$$

where $\gamma = \frac{4}{3} N_A \pi^{3/2} R_0^3$ is a parameter that depends on the probability for cross-relaxation through the donor–acceptor distance for effective transfer R_0 and acceptor concentration N_A, τ_{rad} is the radiative lifetime, and τ_D depends on the interaction and acceptor and donor concentration [16].

According to Eq. (10), the measured room-temperature effective lifetimes were found to be 228, 145 and 128 μs for the 1, 2 and 3 at% samples, respectively. The measured effective lifetime (228 μs) for

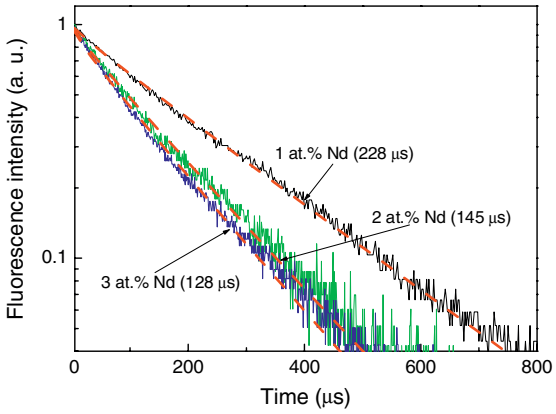

Fig. 3 (online colour at: www.pss-a.com) Emission signal detected at 1.064 μm after excitation by a 5-ns pulse at 808 nm at room temperature for the different concentration Nd^{3+}-doped Nd:YAG crystals. The experimental data are represented by the very thin line. The effective lifetime of 228 μs, 145 μs and 128 μs are fitted with Eq. (10) in the thick dashed lines.

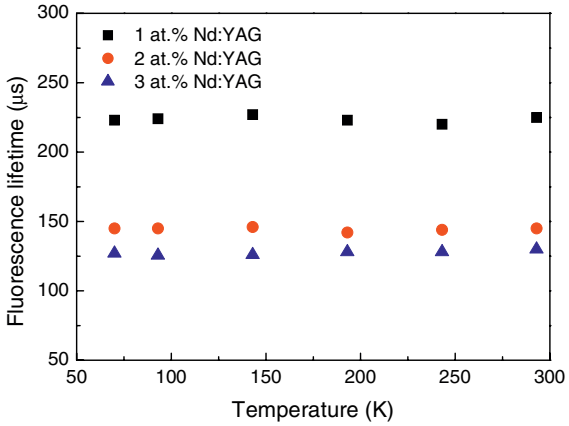

Fig. 4 (online colour at: www.pss-a.com) Variation of the fluorescence lifetime of Nd:YAG crystals doped with different concentrations of Nd with temperature.

1 at% Nd-doped YAG crystal is still shorter than that predicted by the Judd–Ofelt model (Table 4). The measured effective lifetimes of 2 and 3 at% Nd:YAG crystal are shorter than that of 1 at% Nd:YAG crystal. There is concentration quenching in the highly doped Nd:YAG crystals. The energy loss will increase with the concentration increase in highly doped Nd:YAG crystals, there is about 8.8%, 41% and 49% loss for 1, 2 and 3 at% Nd:YAG crytals. The variation of the measured lifetimes with concentration can be related to the nonradiative Nd–Nd relaxation processes relation:

$$\tau_{\text{eff}}^{-1} = \tau_{\text{R}}^{-1} + W_{\text{Nd-Nd}}, \tag{11}$$

where τ_{eff} the measured the fluorescence lifetime is, τ_{R} is the radiative lifetime of Nd:YAG crystal, $W_{\text{Nd-Nd}}$is the nonradiative Nd–Nd quenching probability. The nonradiative Nd–Nd quenching probabilities for 1, 2 and 3 at% Nd^{3+}-doped Nd:YAG crystals are calculated to be 385 s^{-1}, 2896 s^{-1} and 3812 s^{-1}, respectively.

The measured effective fluorescence lifetimes are plotted as a function of temperature in Fig. 4 for each concentration where it is clear that they are independent of temperature. However, the measured lifetime decreases with increasing concentration. The lifetime of the $^4F_{3/2}$ state of Nd^{3+} ions in highly doped Nd:YAG crystals should be governed by the sum of probabilities for several competing processes such as radiative decay, nonradiative decay by multiphonon emission and energy transfer to other Nd^{3+} ions. Judd–Ofelt analysis allows us to assume that the purely radiative lifetime, τ_{R}, of the $^4F_{3/2}$ state is independent of Nd^{3+} concentration, as seen in Table 4. Comparing the lifetimes calculated by the Judd–Ofelt theory with those we measured shows that the measured lifetime of 1 at% Nd^{3+}-doped YAG crystal is still shorter than that calculated for the radiative lifetime. As a result, we use this calculated value as the radiative lifetime to calculate the stimulated emission cross section at different temperatures for all three samples when using the Fuchtbauer–Ladenburg formula [13]:

$$\sigma_{\text{em}}(\lambda) = \frac{1}{8\pi} \cdot \frac{\lambda^5}{n^2 c\tau} \cdot \frac{I(\lambda)}{\int I(\lambda)\lambda \, \mathrm{d}\lambda}, \tag{12}$$

where τ is the radiative lifetime of the upper laser level, c is the light velocity in vacuum, and n is the refractive index at the emission wavelength, ~1.82, and $I(\lambda)$ is the corrected emission spectral intensity as a function of wavelength. Figure 5 shows the fluorescence spectra of the 2 at% Nd:YAG crystal at different temperatures. The emission strength decreases with decrease of the temperature, there is about only one third of that at room temperature especially at 77 K.

The variation with temperature of the stimulated emission cross section of the studied Nd:YAG crystals calculated from our data using Eq. (12) is given in Fig. 6. The results show that the stimulated emission cross section is nearly independent of Nd^{3+} concentration. The dependence of the emission cross section on the temperature will have a significant effect on the laser performance of Nd:YAG-based high-power solid-state laser systems. Rapaport et al. [17] predicted the variation of the stimulated emis-

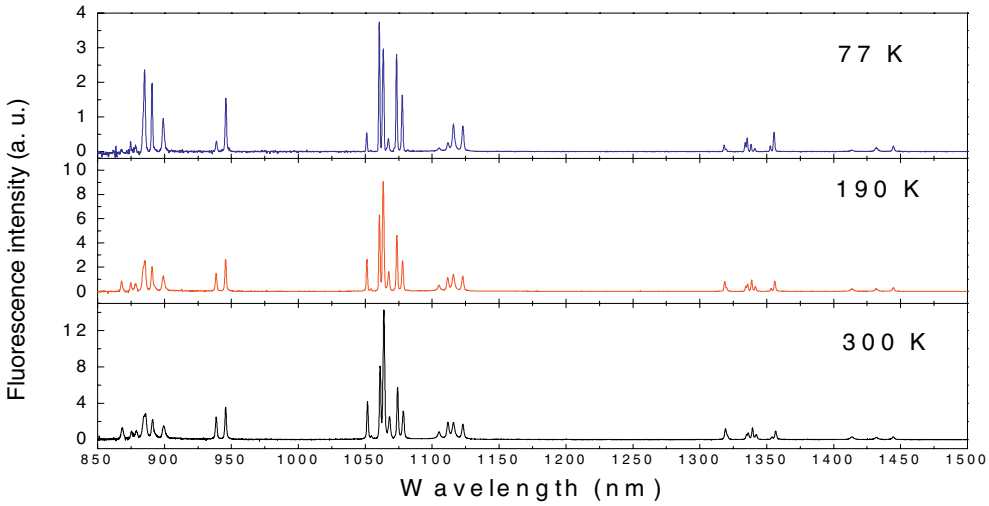

Fig. 5 (online colour at: www.pss-a.com) Fluorescence spectra of 2 at% Nd:YAG at different temperatures.

sion cross section of Nd:YAG crystal with temperature, as a linear function. They measured the stimulated emission cross section of 1 at% Nd:YAG between 203 K and 343 K. Our results extend their results to the temperature range from 70 K to 350 K. As shown in Fig. 6, our temperature-dependent stimulated emission cross section data give a linear relationship as a function of temperature with a negative slope of 3.9×10^{-22} cm^2/K.

4 Conclusions

The emission spectra and lifetime of Nd^{3+} doped YAG crystals with 1, 2 and 3 at% Nd concentrations were measured in the temperature range from 70 K to 300 K. The results show that the measured emission lifetime of Nd^{3+}-doped YAG crystal is independent of temperature though it decreases with Nd^{3+} concentration as a result of concentration quenching. The loss will increase with the increase of concentration in Nd:YAG crystal. There is about 49% loss for 3 at% Nd:YAG crystal. Increasing temperature causes the emission cross section of Nd^{3+}-doped YAG crystals to decrease. Further, the measured temperature-dependent stimulated emission cross sections of the Nd:YAG crystals studied have a linear relationship with temperature. It is now possible to use such a linear relationship between emission cross section and temperature to predict the stimulated emission cross sections between liquid nitrogen and 350 K or above. These results are useful for designing high-power and high-energy Nd:YAG lasers.

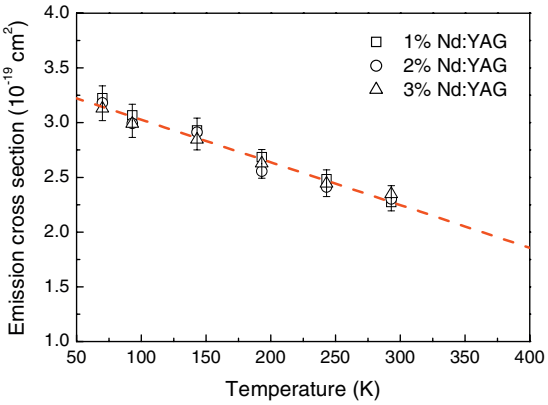

Fig. 6 (online colour at: www.pss-a.com) Stimulated emission cross section as a function of temperature for the differently doped Nd:YAG crystals. The data are indicated and the straight line is the linear fit.

Acknowledgements The authors would like to thank Prof. P. Deng of the Shanghai Institute of Optics and Fine Mechanics, Chinese Academy of Sciences, for providing the Nd-doped Nd : YAG samples.

References

[1] T. Taira, A. Mikai, Y. Nozawa, and T. Kobayashi, Opt. Lett. **16**, 1955 (1991).
[2] P. Gavrilovic, M. S. O'Neill, K. Meehan, J. H. Zarrabi, S. Singh, and W. H. Grodkiewicz, Appl. Phys. Lett. **60**, 1652 (1992).
[3] P. Gavrilovic, M. S. O'Neill, J. H. Zarrabi, S. Singh, J. E. Williams, W. H. Grodkiewicz, and A. Bruce, Appl. Phys. Lett. **65**, 1620 (1994).
[4] I. Shoji, S. Kurimura, Y. Sato, T. Taira, A. Ikesue, and K. Yoshida, Appl. Phys. Lett. **77**, 939 (2000).
[5] J. Lu, M. Prabhu, J. Xu, K. Ueda, H. Yagi, T. Yanagitani, and A. A. Kaminskii, Appl. Phys. Lett. **77**, 3707 (2000).
[6] J. Dong, P. Deng, F. Gan, Y. Urata, R. Hua, S. Wada, and H. Tashiro, Opt. Commun. **197**, 413 (2001).
[7] B. R. Judd, Phys. Rev. **127**, 750 (1962).
[8] G. S. Ofelt, J. Chem. Phys. **37**, 511 (1962).
[9] W. B. Fowler and D. L. Dexter, Phys. Rev. **128**, 2154 (1962).
[10] A. A. Kaminskii, Laser Crystals (Springer, Berlin, 1990).
[11] G. Gashurov and O. J. Sovers, J. Chem. Phys. **50**, 429 (1969).
[12] M. Klintenberg, S. Edvardsson, and J. O. Thomas, Phys. Rev. B **55**, 10369 (1997).
[13] B. F. Aull and H. P. Jenssen, IEEE J. Quantum Electron. **QE-18**, 925 (1982).
[14] I. Garcia-Rubio, J. A. Pardo, R. I. Merino, R. Cases, and V. M. Orera, J. Lumin. **86**, 147 (2000).
[15] H. G. Danielmeyer, B. Blatte, and P. Balmer, Appl. Phys. **1**, 269 (1973).
[16] M. J. Weber, Phys. Rev. B **30**, 2932 (1971).
[17] A. Rapaport, S. Zhao, G. Xiao, A. Horward, and M. Bass, Appl. Opt. **41**, 7052 (2002).